Phase conjugation in critical microemulsions

E. Freysz, E. Laffon, J. P. Delville, and A. Ducasse
Centre de Physique Moleculaire, Universite de Bordeaux 1, 351 Cours de la Liberation, F-33405 Talence Cedex, France
(Received 3 May 1993)

We present a model to describe degenerate four-wave mixing in critical binary liquid mixtures and we analyze it through an experimental study of phase conjugation in critical microemulsions. The two concentration gratings related to the four-wave-mixing configuration give contributions to the conjugated signal which can be separated from their different formation and relaxation times. The model quantitatively describes the amplitude and the dynamics of the gratings and thus of the conjugate signal when one approaches the critical point. The theoretical predictions fit very well with the experimental data. Close to the critical point a 10% reflectivity has been obtained in this medium using a beam power of 1 W from a cw Ar^+ laser. The limitations of these reflectivities at higher powers are discussed.

PACS number(s): 64.60.Fr, 64.70.Ja, 42.65.Hw

Nonlinear optical techniques have been proved to be an interesting tool to characterize the critical behavior of liquid mixtures. Forced Rayleigh scattering (FRS) experiments, for instance, have been performed to analyze the critical properties of laser-induced concentration gratings in such media [1,2]. The increase of the grating reflectivity and the slowing down of the medium response time when approaching a critical point have been explained in terms of critical behavior of both the osmotic compressibility and the correlation length of the concentration fluctuations. These results have been successfully compared to those of classical light scattering [1,2]. In fact, different mechanisms of wave-medium coupling can be responsible for the induced concentration modulations in liquid mixtures. It has been demonstrated in recent years, for example, that a thermal grating gives rise to a concentration grating due to thermodiffusion [1]. Besides, it has been suggested that electrostrictive processes can also induce sizable concentration gratings in binary mixtures [3]. Using microemulsions as particular mixtures, we have previously demonstrated by self-focusing experiments that both thermodiffusion and electrostriction have to be simultaneously taken into account in order to explain the behavior of the very large nonlinearities observed in the vicinity of a critical point [4,5].

More recently, we have performed a degenerate four-wave-mixing (DFWM) experiment to separate the electrostrictive from the thermodiffusive contributions [6]. In this experiment the main idea was to use the simultaneous excitation of two gratings characterized by spatial wave vectors of different amplitudes. Since thermodiffusion is a nonlocal process in contradiction to electrostriction which is local in behavior [5], the two contributions have different wave-vector dependences. The separation of the reflectivities of the two gratings by means of their different response times can then lead to the evaluation of both contributions. However, the theoretical interpretation of the experimental data is difficult if one considers both electrostrictive and thermodiffusive contributions for each grating since their wave-vector dependences and critical behaviors are completely different.

We propose in this paper a quantitative model to describe DFWM in a critical binary liquid mixture. The critical increase of electrostriction is related to that of the osmotic compressibility characterized by a $\gamma=1.24$ exponent while the critical increase of thermodiffusion is characterized by a $\nu=0.63$ exponent (Ising model $n=1$, $d=3$) [5]. Thus, close enough to the critical point, the electrostrictive process always overcomes thermodiffusion. The measure of the reflectivities of both gratings when approaching a critical point results then in a separate determination of the critical behaviors of electrostriction and thermodiffusion. Moreover, the analysis of the formation and relaxation dynamics of the gratings leads to the critical exponent ν of the correlation length of the concentration fluctuations. We next report on the comparison between these theoretical predictions and experimental data obtained in a particular micellar phase of microemulsion.

On the other hand, due to the high value of the nonlinear index of refraction of critical liquid mixtures close to their critical point, these systems can be considered to be interesting materials for phase-conjugate mirror applications. We show in this paper that reflectivities up to 10% can be experimentally achieved in a critical microemulsion. The limitation of this reflectivity related to the wave vector of the induced gratings is theoretically and experimentally analyzed. However, we show that at high laser input powers other limitations have to be taken into account. The possibility of destructive effects on gratings due to convective processes and spinodal decomposition is discussed.

The model proposed to describe DFWM in a critical binary liquid mixture is presented in the first part of the paper. In the second part we present the experimental results and discuss them with respect to the model previously developed.

I. THEORY OF DFWM IN A CRITICAL BINARY LIQUID MIXTURE

Figure 1 presents the basic configuration of our phase conjugation experiment. Two counterpropagating pump

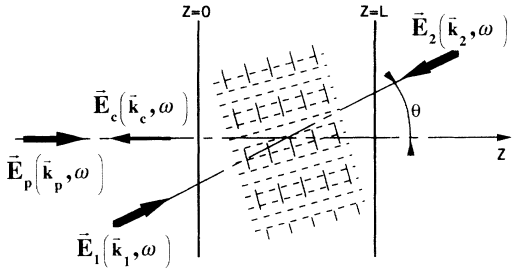

FIG. 1. Basic geometry of phase conjugation via degenerate four-wave mixing.

beams $\mathbf{E}_1$, $\mathbf{E}_2$, and one probe beam $\mathbf{E}_p$ at an angle θ with respect to the pump direction intersect each other in the center of the cell containing a critical binary mixture. All beams are supposed to be monochromatic at the same circular frequency ω and linearly polarized in the same direction. In this configuration each pump wave interferes with the probe beam and creates a modulation of the optical intensity expressed by

$$|\mathbf{E}|^2=\frac{nc_1}{2\pi}\sum_{i=1}^{2}\{|\mathbf{E}_i|^2+|\mathbf{E}_p|^2 +2|\mathbf{E}_i||\mathbf{E}_p|\cos[(\mathbf{k}_i-\mathbf{k}_p)\cdot\mathbf{r}]\}\ , \tag{1}$$

where $(\mathbf{E}_i,\mathbf{E}_p)$, $(\mathbf{k}_i,\mathbf{k}_p)$ are, respectively, the amplitudes and the wave vectors of the pump and probe beams, c_1 and n are the light velocity in vacuum and the linear part of the refractive index of the medium. Each couple $(\mathbf{E}_1,\mathbf{E}_p)$ and $(\mathbf{E}_2,\mathbf{E}_p)$ induces a refractive-index grating by thermal and concentration modulations. The one created by $(\mathbf{E}_1,\mathbf{E}_p)$ [respectively $(\mathbf{E}_2,\mathbf{E}_p)$] reflects the pump beam $\mathbf{E}_2$ [respectively $\mathbf{E}_1$] and gives rise to the conjugated beam $\mathbf{E}_c$ that, in agreement with energy and momentum conservation, is characterized by the same circular frequency ω and the wave vector $\mathbf{k}_c=\mathbf{k}_1+\mathbf{k}_2-\mathbf{k}_p=-\mathbf{k}_p$. The probe, pump, and conjugated beams will be expressed as

$$\mathbf{E}_{p,i,c}=\tfrac{1}{2}\{\mathbf{E}_{p,i,c}\exp[i(\omega t-\mathbf{k}_{p,i,c}\cdot\mathbf{r})]+\text{c.c.}\}\ . \tag{2}$$

To simplify our analysis we will restrict ourselves to the plane wave approximation. The dynamics of the induced concentration gratings can be obtained by solving the mass diffusion equation in the medium, including the electrostrictive and the thermodiffusive contributions [7]. If C_E is the field-induced variation of concentration, this equation reads

$$\frac{\partial C_E}{\partial t}=D_m\left[\nabla^2 C_E+\frac{k_T}{T_0}\nabla^2 T_E-AK_T\nabla^2|\mathbf{E}|^2\right]\ . \tag{3}$$

D_m is the mass diffusivity, and T_0 and T_E are, respectively, the temperature of the medium in absence of field and its field-induced temperature variation. k_T and K_T are, respectively, the thermodiffusive ratio and the osmotic compressibility of the binary mixture. A is a characteristic constant of the medium [7]. The behavior of T_E is governed by two contributions, the thermal diffusivity and a driving term proportional to the heat Q resulting from the weak absorption of the wave in the medium:

$$\frac{\partial T_E}{\partial t}=D_{\text{th}}\nabla^2 T_E+\frac{Q}{\rho_0 C_p}\ . \tag{4}$$

ρ_0, C_p, and D_{th} are, respectively, the initial mass density, the heat capacity at constant pressure, and the thermal diffusivity. In Eqs. (3) and (4) we have neglected the dynamic coupling between concentration and temperature (Duffour effect) that is usually small in liquid mixtures [8]. Q is proportional to the intensity of the field $|\mathbf{E}|^2$ and to the absorption coefficient $\alpha[Q=(\alpha/4)|\mathbf{E}|^2]$.

The general solution of those equations in the case of a critical binary mixture will be described elsewhere. Here we will simplify the treatment and we will only keep the relevant terms with respect to a DFWM experiment. Mass and thermal diffusivities are several orders of magnitude apart in binary liquid mixtures. Even close to a critical point, thermal equilibrium is reached in very short time compared to the characteristic time resulting from mass diffusivity. Since we are interested in the dynamics of C_E, we will suppose then in the following that T_E adapts itself instantaneously to the evolution of $|\mathbf{E}|^2$. Using Eqs. (4) and (5), we obtain the following temperature equation:

$$D_{\text{th}}\nabla^2 T_E+\frac{\alpha|\mathbf{E}|^2}{4\rho_0 C_p}=0\ . \tag{5}$$

We suppose that the two orthogonal gratings are weak enough to be separately treated in first approximation. The Fourier resolution of Eq. (5) gives then the amplitude of the temperature modulation induced by each interference pattern:

$$T_E(q_i)=\frac{\alpha|\mathbf{E}(q_i)|^2}{4D_{\text{th}}q_i^2\rho_0 C_p}\ , \tag{6}$$

where $\mathbf{q}_i=\mathbf{k}_i-\mathbf{k}_p$, $q_i=|\mathbf{q}_i|$, and $|\mathbf{E}(q_i)|^2=2|\mathbf{E}_i||\mathbf{E}_p|$. Inserting Eq. (6) in the stationary limit of Eq. (3), we find the stationary value of the induced concentration variation as a function of the two orthogonal wave vectors $q_{1,2}$:

$$C_E(q_i)=\left[\frac{-\alpha k_T}{4T_0 D_{\text{th}}q_i^2\rho_0 C_p}+AK_T\right]|\mathbf{E}(q_i)|^2\ . \tag{7}$$

Since K_T and k_T are independent of q_i far from a critical point, one can notice that only the thermodiffusive contribution (proportional to k_T) is wave-vector dependent. The dynamic behavior of C_E is obtained when one considers that the probe beam is suddenly applied at time $t=0$ for a duration $\mathcal{T}$:

$$C_E(q_i,0<t'<\mathcal{T})=C_E(q_i)[1-\exp(-t'/\tau_i)]$$
$$C_E(q_i,t'>\mathcal{T})=C_E(q_i)[1-\exp(-\mathcal{T}/\tau_i)]\times\exp[-(t'-\mathcal{T})/\tau_i]\ , \tag{8}$$

where $\tau_i=1/(D_m q_i^2)$. In usual DFWM experiments θ is small. The two wave vectors are then very different ($q_1 \ll q_2$) and some remarks can be made from Eqs. (6)–(8). First, the thermodiffusive contribution for the q_2 concentration grating is negligible compared to that of q_1 since thermal modulations are very small at this wave vector. Besides, the formation and relaxation times τ_2 of this grating are also small compared to those associated to q_1 concentration grating.

Close to a critical point, the variations of the medium parameters are governed by scaling laws including the divergence of some basic properties. For instance, when the critical point is approached by changing the temperature, the osmotic compressibility and thermodiffusive constant have a critical increase described by [2,9,10]

$$K_T(q)=K_T^0\frac{t^{-\gamma}}{1+q^2\xi^2}\ ,$$
$$k_T=k_T^0 t^{-\nu}\ , \tag{9}$$

where t is the reduced temperature related to the critical temperature T_c by $t=(T_c-T)/T_c$. ξ is the correlation length of the concentration fluctuations which diverges according to

$$\xi=\xi_0 t^{-\nu}\ , \tag{10}$$

where ξ_0, K_T^0, and k_T^0 are characteristic constants of the binary mixture. The critical exponents γ and ν are, respectively, equal to 1.24 and 0.63 since critical binary mixtures belong to the universality class described by the Ising model $d=3, n=1$. The behavior of k_T with respect to $q\xi$ is unknown to our knowledge and we will neglect it in this paper. This last assumption is not really restrictive since an important thermodiffusive contribution is only expected at a small wave vector for which the thermal effect is well developed. Then the product $q\xi$ is small at distances (T_c-T) from the critical point currently used in our experimental situations and the corrections with respect to $q\xi$ are slight.

Close enough from the critical point, the formation and relaxation time τ of the induced concentration grating q is also expected to present an original behavior. According to the Kawazaki scaling theory [11]

$$\tau^{-1}=\frac{k_B T}{6\pi\eta}q^3 K(q\xi)\ , \tag{11}$$

where $K(q\xi)$ is the Kawasaki function:

$$K(x)=\tfrac{3}{8}[x^{-1}+x^{-3}+(1-x^{-4})\tan^{-1}(x)]\ . \tag{12}$$

η and k_B are, respectively, the shear viscosity of the fluid and the Boltzmann constant. Note that other parameters are also characterized by a critical behavior. For example, in Eqs. (7)–(12) C_p, $D_{\rm th}$, η diverge. But, since their related critical exponents are small, their critical behaviors can only be expected very close to T_c. They will be neglected since their variations are weak compared to those of K_T, k_T, and τ.

Inserting Eqs. (9) and (10) in Eq. (7), we observe that the induced concentration variation C_E diverges close to a critical point. This behavior is illustrated in Fig. 2. Figure 2(a) shows the evolution of the normalized variation C_E^* when one approaches the critical temperature, for different wave vectors, without thermodiffusive contribution ($k_T=0$). At large wave vectors the rapid increase of the induced concentration variation C_E^* observed far from the critical point ($q\xi \ll 1$) saturates as one gets closer to T_c ($q\xi \gg 1$). This saturation occurs more and more closer to T_c when decreasing q. It is

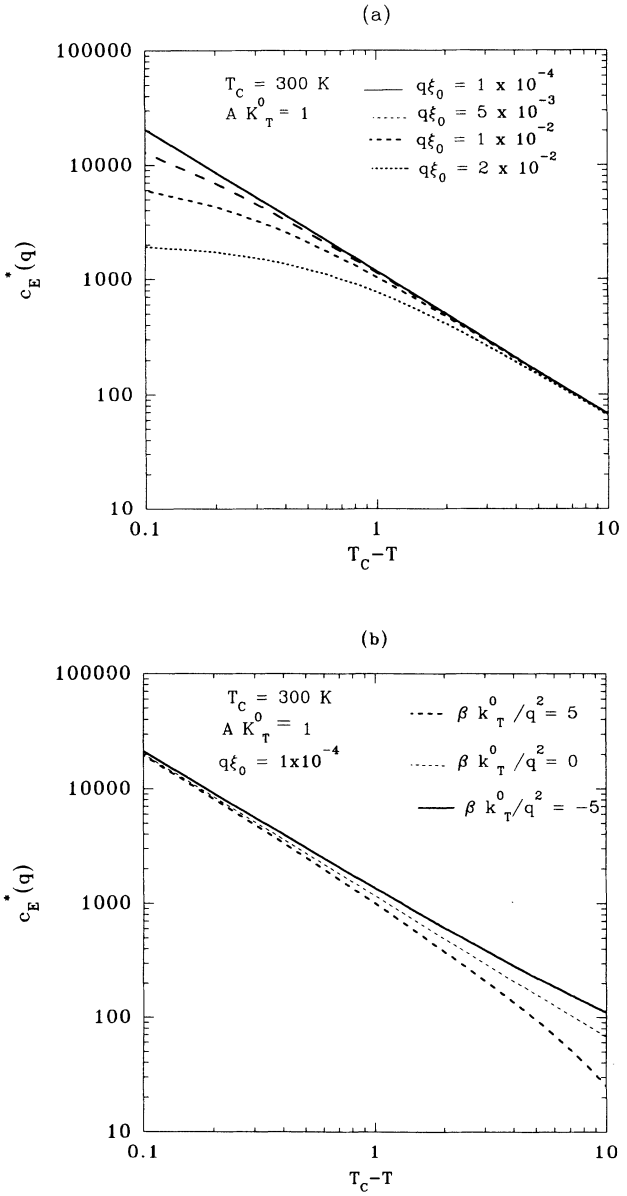

FIG. 2. Temperature dependence for the normalized concentration variation $C_E^*(q_i)=C_E(q_i)/|\mathbf{E}(q_i)|^2$ for $T_c=300$ K, $AK_T^0=1$, $\xi_0=44$ Å. (a) Variation with negligible thermodiffusion. (b) Variation with positive or negative thermodiffusion contribution and comparison with the negligible thermodiffusion case. $\beta=(\alpha/4T_0 D_{\rm th}\rho_0 C_p)$.

negligible in the domain 0.1 K $<(T_c-T)<10$ K for $q\xi_0=10^{-4}$. The result of the thermodiffusive contribution to C_E^* is illustrated in Fig. 2(b) for this small value of q ($q\xi_0=10^{-4}$). According to the sign of the thermodiffusive constant k_T, this contribution increases or decreases the C_E^* value. However, since the critical exponent γ of the osmotic compressibility K_T is larger than the critical exponent ν of k_T ($\gamma\approx 2\nu$), the thermodiffusive effect becomes negligible compared to the electrostrictive one when approaching the critical point. Moreover, the thermodiffusive process is only important at small wave vectors. Due to the q^{-2} dependence in the corresponding term of Eq. (7), it rapidly decreases when q increases. Then, in our experimental conditions, it has to be taken into account only for the large spacing grating q_1 and far from the critical point.

The index or dielectric constant variation induced by the field results, in a general way, from both T_E and C_E variations and can be written as

$$\delta\epsilon(r,\ell)=\frac{\partial\epsilon}{\partial C}C_E(r,\ell)+\frac{\partial\epsilon}{\partial T}T_E(r,\ell)\ . \tag{13}$$

In the following we will mostly be interested in the change of the real part ϵ' of the dielectric constant ($\epsilon=\epsilon'+i\epsilon''$). Since close to a critical point concentration variations C_E are large, we can neglect the small thermal contribution to $\delta\epsilon'$ and write

$$\delta\epsilon'(\mathbf{r},\ell)=\frac{\partial\epsilon'}{\partial C}\sum_{i=1}^{2}C_E(q_i,\ell)\cos(\mathbf{q}_i\cdot\mathbf{r})\ . \tag{14}$$

Inserting Eq. (14) in the classical nonlinear wave equation leads to the coupled propagation equations of all beams involved in the DFWM experiment. We are essentially interested in the evolution of the probe and conjugate beam amplitudes. Since all the beams are considered as plane waves, in the configuration represented in Fig. 1, $\mathbf{E}_p$ and $\mathbf{E}_c$ are independent of the transverse coordinates x and y and only functions of z and ℓ. In the approximation of the slowly variable amplitude, their propagation equations can be written as [12]

$$\begin{aligned}\frac{\partial\mathbf{E}_p(z,\ell)}{\partial z}+\frac{\alpha}{2}\mathbf{E}_p(z,\ell)&=i[\kappa(q_1,\ell)+\kappa(q_2,\ell)]\mathbf{E}_c^*(z,\ell)\ ,\\ \frac{\partial\mathbf{E}_c^*(z,\ell)}{\partial z}+\frac{\alpha}{2}\mathbf{E}_c^*(z,\ell)&=i[\kappa(q_1,\ell)+\kappa(q_2,\ell)]\mathbf{E}_p(z,\ell)\ ,\end{aligned} \tag{15}$$

where $\alpha=\epsilon''\omega/\sqrt{\epsilon'}c_1$, $\kappa(q_i,\ell)=(\omega/2\sqrt{\epsilon'}c_1)[\delta\epsilon'(q_i,\ell)/|\mathbf{E}(q_i)|^2]|\mathbf{E}_1||\mathbf{E}_2|$.

If we first neglect the attenuation of the probe and conjugate beams, the medium reflectivity of the probe beam can be deduced from Eq. (15) [13]:

$$\begin{aligned}R(\ell)&=|E_c(z=0)/E_p(z=0)|^2\\&=\tan^2\{[\kappa(q_1,\ell)+\kappa(q_2,\ell)]L\}\ ,\end{aligned} \tag{16}$$

where L is the useful thickness of the sample. We have plotted in Fig. 3(a) (solid line) the evolution of the static reflectivity $R(\infty)$ in absence of thermodiffusion, when approaching the critical temperature, for small arguments of the tangent [$R(\infty)\ll 1$]:

$$\begin{aligned}R(\infty)&=\{[\kappa(q_1,\infty)+\kappa(q_2,\infty)]L\}^2\\&=\left[\frac{t^{-\gamma}}{1+(q_1\xi_0)^2t^{-2\nu}}+\frac{t^{-\gamma}}{1+(q_2\xi_0)^2t^{-2\nu}}\right]^2(\kappa_0 L)^2\ ,\end{aligned} \tag{17}$$

where κ_0 is the constant prefactor of κ. As expected, we observed a strong increase of $R(\infty)$ due to the divergence of the thermodynamical parameters when (T_c-T) tends to zero. The condition $R(\infty)\ll 1$ is no longer satisfied for the pump power chosen in Fig. 3(a) in the domain $(T_c-T)<0.1$ K. In order to continue satisfying this condition when decreasing (T_c-T), the pump intensities have to be reduced. When approaching the critical point, we have to note that the contribution to the reflectivity of the fine grating q_2 saturates much more rapidly than that of the coarse grating q_1. We expect then to experimentally observe the disappearance of the fine grating contribution as one gets closer to the critical point.

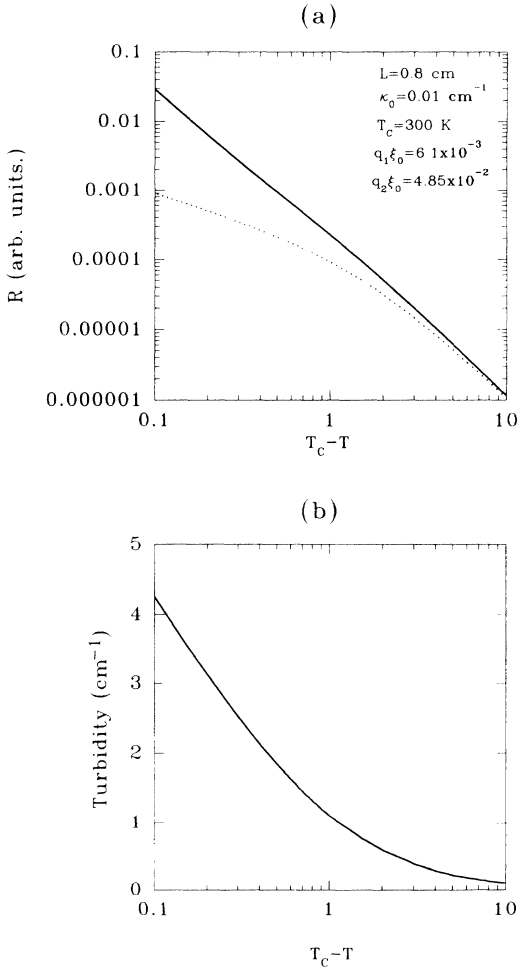

FIG. 3. (a) Evolution of the reflectivity in the weak signal regime in the absence (——) and presence (— — —) of turbidity of the sample. (b) Theoretical evolution of the turbidity with respect to temperature for $\xi_0=44$ Å, $k=1.22\times10^{-7}$ m^{-1}, $\tau_0=0.01$ cm^{-1}, and $T_c=300$ K.

If the pump intensities are kept constant when $(T_c - T)$ tends to zero the tangent argument continuously increases and the approximation of Eq. (17) is no longer valid. Equation (16) shows that $R(\infty)$ diverges when $\{[\kappa(q_1,\infty)+\kappa(q_2,\infty)]L\}=(n+\frac{1}{2})\pi$, with $n=0,\pm1,\pm2,\ldots$. From these successive divergences, it can be expected to experimentally observe oscillations of the reflectivity when one approaches the critical point at constant pump intensities.

Next we consider the influence of the scattering losses on the conjugated signal in critical liquid mixtures. These losses become huge in the vicinity of a critical point, due to the divergence of the correlation length of the concentration fluctuations ξ. The turbidity τ_s of the mixture increases according to the following scaling law [14]:

$$\tau_s=\tau_0 t^{-\gamma}\Gamma(2(k\xi)^2)\,, \tag{18}$$

where $\Gamma(x)$ is a function of the following form: $\Gamma(x)=[(2x^2+2x+1)/x^3]\ln(1+2x)-2(1+x)/x^2$. ξ diverges according to Eq. (10). The divergences of τ_s as a function of (T_c-T) is presented in Fig. 3(b). It results in a saturation of $R(\infty)$. To take into account in Eq. (15) the beam intensity attenuation due to the turbidity, it is worth noticing that the product $\mathbf{E}_1\mathbf{E}_2$ is not dependent on z. $\kappa=\kappa(q_1,\infty)+\kappa(q_2,\infty)$ is then a constant in all the medium. Defining the evolution of $\mathbf{E}_p$ and $\mathbf{E}_c$ by $\mathbf{E}_p(z,t)=\mathbf{E}_p\exp(-\tau_s/2z)$ and $\mathbf{E}_c(z,t)=\mathbf{E}_c\{1-\exp[-\tau_s/2(L-z)]\}$ Eq. (15) yields [13]

$$R(\infty)=\frac{4\kappa^2\exp(-\tau_s L)\tan^2(\kappa' L)}{[2\kappa'+\tau_s\tan(\kappa' L)]^2}\,, \tag{19}$$

where $\kappa'=\sqrt{\kappa^2\exp(-\tau_s L)-(\frac{1}{2}\tau_s)^2}$. The saturation of $R(\infty)$ related to the variation of τ_s given in Fig 3(b) is shown on the dotted line of Fig. 3(a). This demonstrates that scattering losses can be an important limitation to the use of critical media as conjugated mirrors when one approaches the critical point.

II. EXPERIMENTAL RESULTS

The critical mixture used to check the previous theoretical predictions is a critical microemulsion. Water-in-oil microemulsions are stable suspensions of surfactant-coated water droplets called micelles, a few nanometers in diameter, in an oil-rich continuous phase. In this system critical consolute points due to micellar interactions have been discovered and analyzed [15]. Close to the critical consolute point, the system behaves like a critical binary mixture. However, in microemulsions, the critical behaviors are observed far from the critical point since the micelle dimensions are larger than those of classical molecules involved in classical critical binary liquid mixtures (typically 8 nm in diameter in our case compared to a few angstroms). Moreover, if the refractive index of the micelles is different from the index of refraction of the surrounding medium, the size of the micelles confers to such a system a higher polarizability than that of simple binary liquid mixtures. Those characteristics show that a critical microemulsion is a good candidate to obtain a strong reflectivity in a DFWM experiment.

The experimental setup presented in Fig. 4 has been described in a previous paper [6]. Two pump beams of intensities I_1 and I_2 and one probe beam I_p at an angle θ from the pump direction are split off from the 514.5-nm output of a cw Ar^+ laser. The angle θ can be varied from 1° to 20°. In this variation the coarse grating has a period that varies from 30 to 1.5 μm while the period of the fine grating remains nearly constant around the value $\lambda/2=0.22$ μm. The 1-m focal lens forms in the cell a waist of 120 μm in diameter. The probe beam is slowly mechanically chopped and the conjugate wave is detected by means of a photomultiplier and a signal averager. The 2-mm-thick cell contains a four-component microemulsion, whose composition is the following in mass percentages: toluene 70.6%, butanol 16.4%, water 8.9%, sodium dodecyl sulfate (SDS) 4.1%. This mixture presents a critical point at $T_c=33.95$ °C. A rectangular capillary glass tube (thickness 0.3 mm, width 4 mm) is located inside the cell close to the input plane of the probe beam in order to prevent convective effects due to temperature and concentration gradients induced in the mixture as discussed later in this paper. No signal is observed if this capillary is removed. The cell is inserted in a temperature-controlled oven whose temperature stability is ≥ 0.02 °C.

A typical signal obtained when the probe beam is chopped at 3 °C from the critical point is presented in Fig. 5. Two different characteristic times related to the formation and relaxation of the two induced gratings can be evidenced. Since the time constants of the two gratings are far away from each other [for $\theta\approx 7°$, $\tau_1/\tau_2=(q_2/q_1)^2=330$], they cannot be simultaneously resolved in this figure. The formation and relaxation of the fine grating appear instantaneously in this graph. The dots represent experimental data. The solid curve corresponds to a fit of these data with the theoretical curve obtained from Eq. (17) and exponential formation and relaxation of the gratings according to Eq. (8) with a time constant $\tau_1=107$ ms corresponding to the coarse grating q_1 and $\tau_2=0$ corresponding to the fine grating q_2.

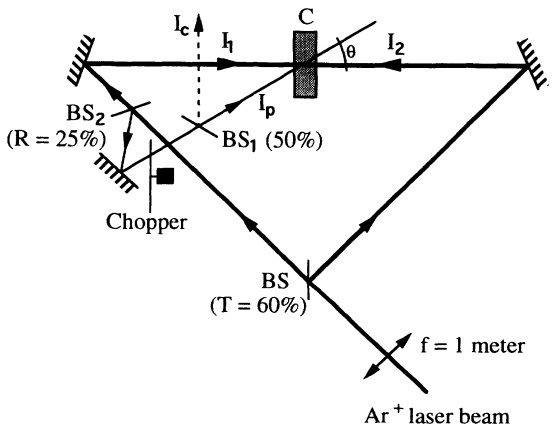

FIG. 4. Schematic diagram of the experimental setup. BS's: beam splitters; C: cell.

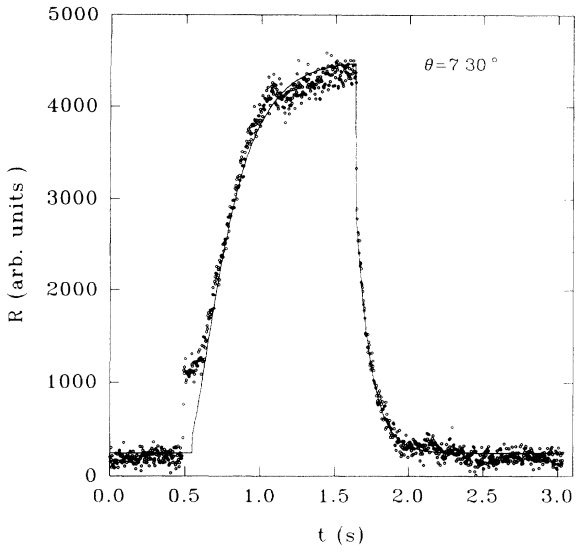

FIG. 5. Typical degenerate four-wave mixing signal at $\theta=7.30°$ with the same pump and probe polarization, pump excitation of duration $T_{exc}=1.1$ s. The solid curve represents a fit according to Eq. (24).

The agreement is good. We can clearly understand this temporal behavior. When the probe beam is applied we first observed a step due to the quasi-instantaneous formation of the fine grating q_2 followed by a slow increase of the reflectivity induced by the formation of the coarse grating q_1. A similar behavior is observed when the probe beam is stopped. The fine grating vanishes rapidly, inducing a step in the reflectivity and after that a slow decrease of the signal is observed due to the slower diffusion of the micelles in the coarse grating. Note, however, that the amplitudes of the two steps related to the formation and the relaxation of the fine grating are different. This is due to the coupling between both gratings involved in Eq. (17). During the formation of the fine grating, the coarse grating is practically absent and the term $2[\kappa(q_1,t)\kappa(q_2,t)]$ is nearly zero. On the other hand, this term is non-negligible during the relaxation of the fine grating.

In order to clearly evidence the contributions of the two concentration gratings to the conjugate wave we have used different configurations of the pump and probe polarizations. The experimental results are presented in Fig. 6 for a small angle θ between the pump and the probe beams. When the fine grating is absent [Fig. 6(b), I_2 polarization perpendicular to I_1 and I_p polarizations], only the effect of the coarse grating with a large time constant is observed. If the coarse grating is absent [Fig. 6(c), I_1 polarization perpendicular to I_2 and I_p polarizations] we observe only a fast contribution. No signal except a weak noise due to the scattering of the probe beam is observed when no useful grating is induced in the sample [Fig. 6(d), I_p polarization perpendicular to I_1 and I_2 polarizations]. Besides, these results show clearly that contributions of the thermal gratings to the conjugate wave are very small.

Next, to probe the linearity of the medium response with respect to the intensities of the pump beams, we have measured the amplitude variations of the signal as a function of the total laser intensity. In our experimental configuration, we expect to observe an increase proportional to the cube of the total laser intensity. A typical experimental result is presented in Fig. 7 at 10°C from the critical temperature. At low power the data are in good agreement with the expected behavior. However, at larger intensity a systematic deviation with respect to this behavior is always observed. This discrepancy cannot be attributed to the oscillatory behavior of $R(\infty)$ given by Eq. (16) since the experimental reflectivity remains much smaller than 1. Then the development of Eq. (17) is al-

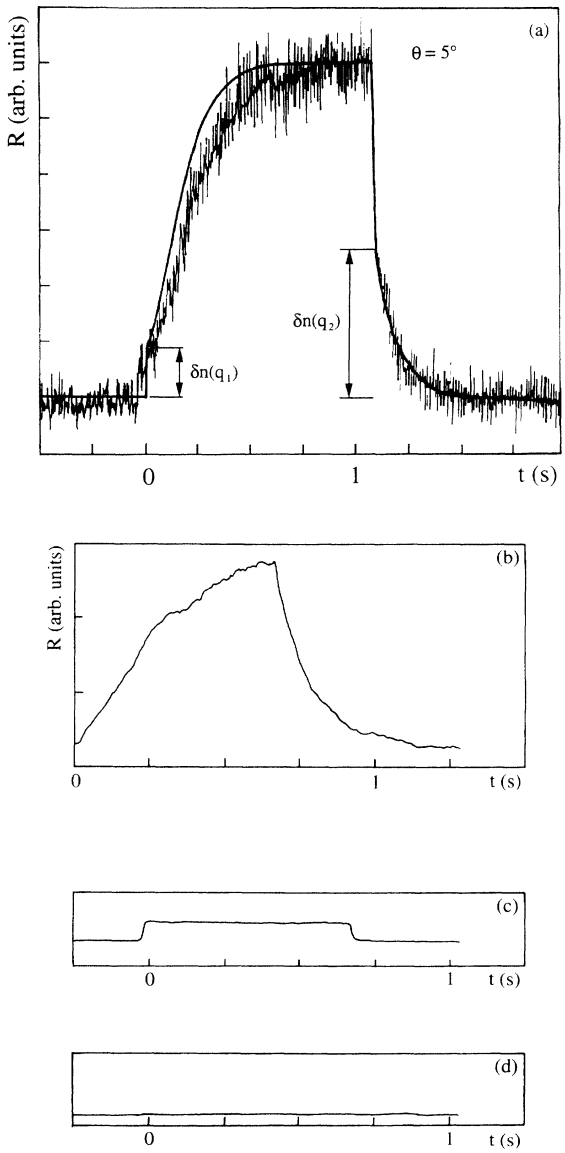

FIG. 6. (a) DFWM at $\theta=5°$ with the same pump and probe polarizations. (b), (c), (d) Same evolution with orthogonal polarization of one of the three beams: (b) the backward pump beam, (c) the forward pump beam, (d) the probe beam.

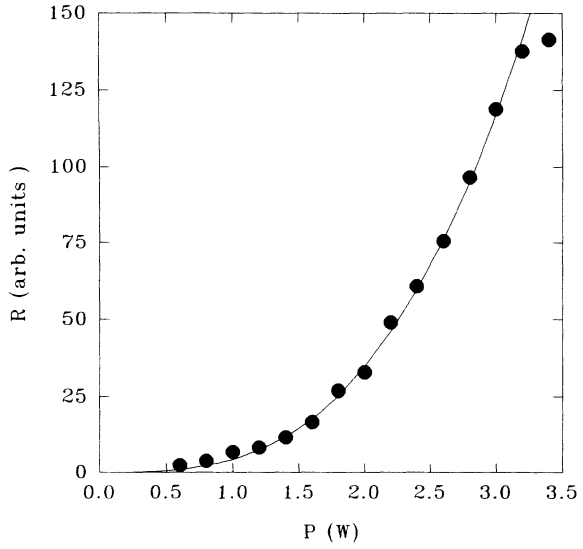

FIG. 7. Evolution of the intensity of the reflected wave as a function of the total laser power. The solid curve is a fit assuming a cubic dependence.

ways valid. It could be instead due to convective motions occurring in the mixture when concentration gradients are large enough as discussed below. Close to the critical point this phenomenon is observed at lower power: less than 1.5 W at 0.3 °C to the critical temperature.

We have also analyzed the temperature behavior of the reflectivity when we approach the critical temperature. In order to avoid any nonlinearity of the medium response with respect to the beam intensities, the total laser power was kept below 1 W. The angle θ was fixed at 7.30°. The comparison of Figs. 8(a) and 8(b) demonstrates that, due to the divergence of ξ, the fine grating q_2 saturates farther from the critical point than the coarse grating q_1. The instantaneous contribution of the fine grating which is important at 5 °C from T_c [Fig. 8(a)] has almost disappeared at 0.5 °C from T_c [Fig. 8(b)]. From such a set of data we can study the critical evolution of both gratings. However, since the contribution to the signal of the fine grating is less and less important as one approaches the critical point, a quantitative analysis of this contribution remains difficult. On the other hand, we can quantitatively analyze the contribution of the coarse grating to the reflectivity. This is presented in Fig. 9. As expected, we observe a huge increase of the reflectivity when T tends to T_c: the reflectivity increases by more than three orders of magnitude. In order to compare these data with our model, we have to introduce the turbidity of our sample [Eq. (18)]. Turbidity measurements had been previously carried out and will be published elsewhere. Using these values of turbidity and other relevant parameters of our sample ($\xi_0=44$ Å, $\nu=0.63$, $\gamma=1.24$),only one adjustable parameter is needed to fit measurements with theoretical predictions given by Eqs. (7), (9), and (10). A multiplying factor is chosen so that the theoretical reflectivity is equal to the experimental one at 29.4 °C. This fit of the variations of the reflectivity square root as a function of temperature [16], taking into account only the contribution of the coarse grating, is presented in an inset of Fig. 9. The solid curve presents the theoretical variation, dots are the experimental data. A very good agreement is observed. Note, however, that the closest point from the critical temperature deviates appreciably from the theoretical curve. This indicates that not all of the relevant processes are taken into account very close to the critical point. Concerning the dynamics of the conjugated signal, we have plotted in Fig. 10 the evolution of the coarse grating relaxation with temperature. We observe a divergence of the relaxation time τ_1 when T tends to T_c. This time constant increases from 0.036 s at 8 ° C from the critical point to 0.43 s at 0.3 °C from the critical point. In the same graph we report the fit obtained from Eq. (11) using the following variation of viscosity $\eta(T)=(0.019T+7.121)10^{-2}$ poise (T in K) [2]. We observe a good agreement of the fit with our experimental data. Note, moreover, that we have no adjustable parameter in this fit.

Finally, we have analyzed the behavior of the

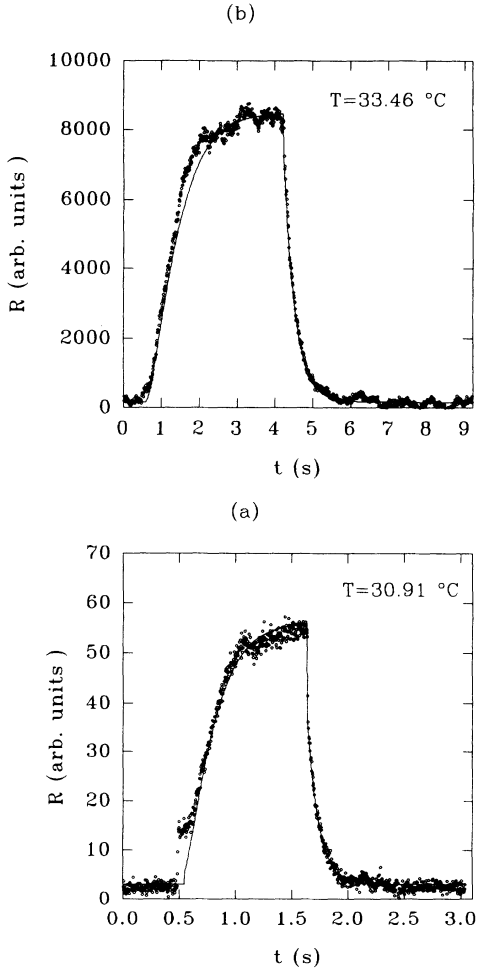

FIG. 8. Evolution of the DFWM signal when approaching the critical point for $\theta=7.30°$. (a) Large contribution of the fine grating at 5 °C from T_c. (b) Negligible contribution of the fine grating at 0.5 °C from T_c.

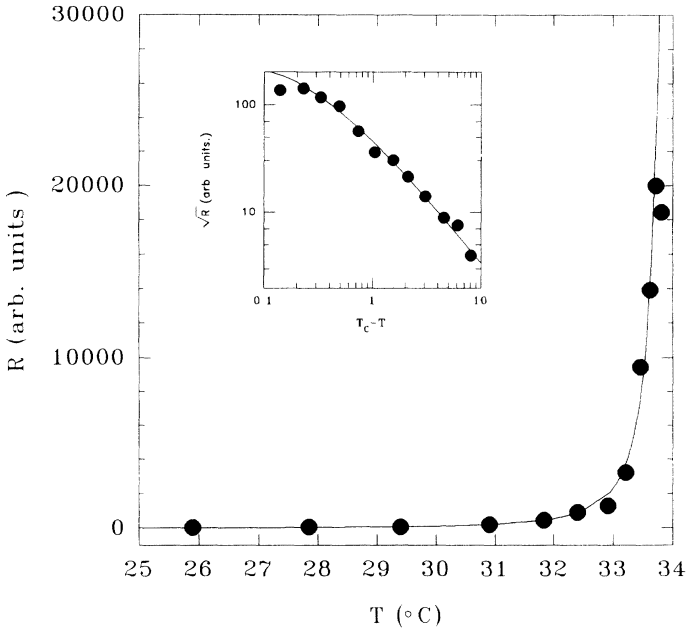

FIG. 9. Evolution of the coarse grating contribution to the reflectivity under steady-state pump excitation when approaching the critical point. The solid curve is a fit according to Eq. (27) with one free parameter. The inset presents the evolution of the square root of the reflectivity as a function of T in logarithmic coordinates. The curve is obtained from the proportionality of this function to K_T and from the divergence of K_T given by Eq. (10).

reflectivity when one increases the pump and probe beam powers beyond the domain where the medium response is linear. Far from the critical point, we observed saturation of the reflectivity to values of the order of a few percent. At 0.15 °C from the critical point, the reflectivity saturates at about 10% and then rapidly decreases as we further increase the laser power. The conjunction of two different processes could be responsible for such an observation. First, as we increase the total laser beam power the temperature and concentration variations of the sample can drive the system beyond the critical point and induce a phase separation [17] through a spinodal decomposition which blurs the gratings. On the other hand, convective instability in our cell can limit the amplitude

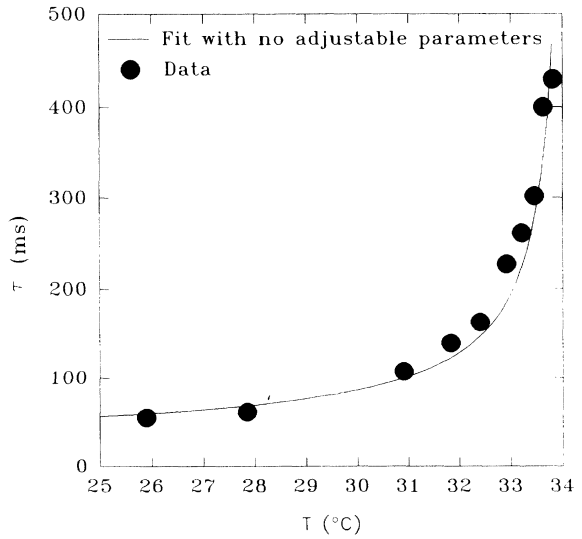

FIG. 10. Evolution of the relaxation time of the coarse grating when approaching the critical point. The solid curve is a fit from Eq. (14) with no adjustable parameters.

of the concentration grating, as we have already mentioned. Indeed, if in simple fluids an unstable situation is only associated to the thermal expansion of the density, in binary fluid mixtures, density may also vary with the concentration. This second mechanism, which is divergent at the critical point, is often dominant in mixtures and can lead to an important decrease of the convective threshold. By analyzing its critical behavior, it is possible to evaluate at which distance from the critical point it becomes important. According to [18], for a mixture layer of thickness d, convection develops if the Rayleigh number R_c related to the concentration gradient ∇C is larger than 720:

$$R_c=\frac{\rho_0 g\beta d^4\nabla C}{D_m\eta}\geq 720\ , \tag{20}$$

where g is the acceleration due to gravity and $\beta=1/\rho_0(\partial\rho/\partial C)$. Since ∇C diverges in the vicinity of the critical point and $D_m=D_m^0 t^{\nu}$ the Rayleigh number R_c also diverges. When contribution to ∇C is mainly electrostrictive, R_c behaves as $t^{-(\nu+\gamma)}$ ($R_c\propto t^{-2\nu}$ in the thermodiffusive case). Typically in our system for an incident beam power of 25 mW per fringe (laser beam power $P=1$ W and $\theta=7.30°$) and $d=60$ μm, the electrostrictive gratings are progressively destroyed by the convective flux when $(T_c-T)\leq 1$ K. This shows the drastic increase of the convective processes close to the critical point and qualitatively explains the observed deviation of the reflectivity from the theoretical curve as we increase the laser power. In the same conditions, the thermodiffusive contribution to convection is negligible since instabilities develop only when $(T_c-T)\leq 4\times 10^{-2}$ K.

In conclusion we have developed a quantitative model to describe DFWM in critical binary liquid mixtures and, as an example, we have experimentally analyzed the cw phase-conjugate signal obtained with a critical mi-

croemulsion using a cw Ar^+ laser. Experimental data are well described by our model except at high laser powers and very close to the critical point where perturbations induced by the waves prevent a simple quantitative analysis. In particular, the critical increase of the reflectivity and the relaxation time obeying the predicted scaling laws have been observed. A reflectivity up to 10% and a critical slowing down up to one order of magnitude have been achieved. Besides, it should be kept in mind that this method could be an interesting tool to quantitatively characterize critical mixtures. For instance, it is well known that single-scattering Rayleigh cross sections are difficult to obtain near the critical point by classical light-scattering techniques, due to multiple-scattering problems, in the domain where the turbidity is very high. Since the conjugate signal is proportional to the square of the single-scattering Rayleigh cross section, this paper demonstrates that this parameter can be obtained from DFWM experiments if the turbidity of the sample is correctly taken into account.

ACKNOWLEDGMENT

The Centre de Physique Moleculaire is "associé au Centre National de la Recherche Scientifique."

[1] D. W. Pohl, Phys. Lett. **77A**, 53 (1980); in *Proceedings of the Conference on Light Scattering in Liquids and Macromolecular Solutions,* edited by V. Degiorgio, M. Corti, and M. Giglio (Plenum, New York, 1980).

[2] E. Freysz, W. Claeys, A. Ducasse, and B. Pouligny, IEEE J. Quantum Electron. **QE22**, 1258 (1986).

[3] F. V. Bunkin, G. A. Lyakov, K. F. Shipilov, and T. A. Shmaonov, Pis'ma Zh. Eksp. Teor. Fiz. **35**, 251 (1982) [JETP Lett. **35**, 315 (1982)].

[4] E. Freysz, M. Afifi, A. Ducasse, B. Pouligny, and J. R. Lalanne, J. Phys. Lett. **46**, 181 (1985).

[5] B. Jean-Jean, E. Freysz, A. Ducasse, and B. Pouligny, Europhys. Lett. **7**, 219 (1988).

[6] E. Freysz, E. Laffon, and A. Ducasse, Opt. Lett. **16**, 1644 (1991).

[7] B. Jean-Jean, E. Freysz, A. Ponton, A. Ducasse, and B. Pouligny, Phys. Rev. A **39**, 5268 (1989).

[8] K. Thyagarajan and P. Lallemand, Opt. Commun. **26**, 54 (1978).

[9] L. S. Ornstein and F. Zernike, Proc. K. Ned. Akad. Wet. **17**, 793 (1914).

[10] M. Giglio and A. Vendramini, Phys. Rev. Lett. **34**, 561 (1975).

[11] K. Kawasaki, in *Phase Transitions and Critical Phenomena,* edited by C. Domb and M. S. Green (Academic, New York, 1976), Vol. 5A.

[12] E. Freysz, These d'etat, Universite de Bordeaux, 1990.

[13] D. M. Pepper and A. Yariv, in *Optical Phase Conjugation,* edited by R. A. Fisher (Academic, New York, 1983).

[14] V. G. Puglielli and N. C. Ford, Phys. Rev. Lett. **25**, 143 (1970).

[15] J. S. Hang, and M. W. Kim, Phys. Rev. Lett. **47**, 1462 (1981).

[16] In our system the square root of the reflectivity of the large grating is proportional to the osmotic compressibility and should evolve like it.

[17] J. P. Delville, C. Lalaude, E. Freysz, and A. Ducasse, Phys. Rev. E (to be published).

[18] D. Gutkovicz-Krusin, M. A. Collins, and J. Ross, Phys. Fluids **22**, 1443 (1979); **22**, 1451 (1979).

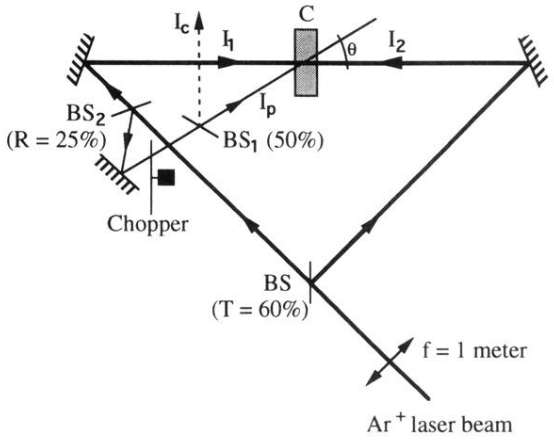

FIG. 4. Schematic diagram of the experimental setup. BS's: beam splitters; *C*: cell.